Check for updates

Micellization, surface activities and thermodynamics study of pyridinium-based ionic liquid surfactants in aqueous solution†

Dong Fu, [ID] [a] Xiaoru Gao,[b] Bo Huang,[a] Jue Wang,[a] Yao Sun,[a] Weijun Zhang,[a] Kan Kan,*[a] Xiaochen Zhang, [ID] *[a] Yang Xie[a] and Xin Sui[a]

The micellization and surface activity properties of long-chain pyridinium ionic liquids n-alkyl-3-methylpyridinium bromide ([$C_n$mpy][Br], n: the carbon numbers of hydrophobic tails, $n = 12, 14, 16$) in aqueous solution were systematically investigated through electronic conductivity measurement, surface tension, and ultraviolet-absorption spectra. The surface chemical parameters and thermodynamics parameters were obtained. The [$C_n$mpy][Br] ionic liquids exhibit higher surface activities than conventional surfactants with corresponding alkyl chain lengths. The effects of inorganic salts (LiBr, NaBr, MgBr$_2$), organic alcohols (C$_2$H$_5$OH, C$_3$H$_7$OH, C$_4$H$_9$OH, C$_5$H$_{11}$OH) and temperature on the critical micelle concentration (CMC) values of [$C_n$mpy][Br] aqueous solutions were also investigated. The CMC values remarkably decreased with the addition of inorganic salts. The CMC values increased slightly in the presence of ethanol, but decreased gradually as the chain length of the alcohol increased. The CMC values assumed a trend of decreasing and then increasing with the increase of temperature. The calculation results of thermodynamic parameters show that both adsorption and micellization processes of [$C_n$mpy][Br] are spontaneous; the enthalpy of [C_{12}mpy][Br] is negative at 293.15 K and becomes negative with temperature increasing. For [C_{14}mpy][Br] and [C_{16}mpy][Br] this transition occurs at 288.15 K and the micellization process is entropy-driven in the investigated temperature range.

1 Introduction

Ionic liquids (ILs), which melt at or close to room temperature, are a class of organic molten electrolytes composed of an organic cation and an inorganic anion. They have been receiving much attention over recent years due to their specific chemical and physical properties such as nonflammability, negligible vapor pressure, low volatility, high thermal stability, high ionic conductivity, and easy recyclability.[1,2] These unique properties make ILs suitable candidates for a large range of applications.[3] ILs bearing long alkyl chains have shown obvious amphiphilic characters and could possess surface active properties similar to the conventional cationic surfactants. Owing to the inherent molecular nature, the long-chain IL molecules can self-assemble in aqueous media to form micelles, vesicles, lyotropic liquid crystals, and gels, *etc.*[4] The self-assembly of ILs make it suitable for a range of application such as liquid–solid extraction,[5] corrosion protection,[6] synthesis of functionalized carbon nanotubes,[7] synthesis of CuO nano-structures,[8] phase-

transfer catalysts,[9] oil recovery,[10] drug/gene delivery systems,[11] dispersants of petroleum asphaltenes,[12] green solvents of carbohydrate,[13] cosmetics[14] and textile industry.[15] Therefore, micellization behavior of ILs has become one of the intriguing objects in the field of colloid and interface chemistry. The analysis of physical and thermodynamic behavior of ILs in aqueous solution is very important to help us comprehend their applicability in different industries.

Micellization behavior of ILs based on the imidazolium, pyrrolidinium, piperidinium has been intensively explored.[16–24] Some papers have reported the aggregation behavior of pyridinium-based ILs in water.[25–27] These researches mainly focused on the *N*-substitution pyridinium and anions. Only few studies on the colloidal chemical aspects of amphiphilic methylpyridinium based ILs were reported.[16,25,28–32] Fayyaz *et al.* synthesized five new surfactants [$C_n$mpy][Br] ($n = 6, 8, 10, 12, 14$) and investigated the micellization behavior of [$C_n$mpy][Br] in ethanol.[33,34] The results showed that [$C_n$mpy][Br] had lower CMC value in ethanol and significant antimicrobial activities. However, the adsorption of [$C_n$mpy][Br] at the air/water interface and the mechanism of micelle formation in water have not yet been investigated.

In this work, we studied the micellization behavior and surface activities of [$C_n$mpy][Br] ($n = 12, 14, 16$) in aqueous solution in detail by conductivity, surface tension and UV

[a]Heilongjiang Academy of Sciences Institute of Advanced Technology, Harbin, 150020, China. E-mail: kankan.has@foxmail.com; xc_zhang.has@hotmail.com

[b]Harbin FRP Research Institute, Harbin, Heilongjiang 150029, China

absorption spectra. In addition, the counterion and alcohol have strong influence on CMC value and shape of the aggregates of the micelle system.[35,36] Thus, we also investigated the effects of the additives (inorganic salts and organic alcohol) on the micellization behavior of $[C_n mpy][Br]$ in aqueous solution. As an extension of the previous study, we also analyzed adsorption and micellization processes of $[C_n mpy][Br]$ aqueous solution through thermodynamic parameters. These thermodynamic parameters were calculated from the temperature dependence of CMC value and the degree of dissociation of micelles (β), which obtained by approach in the conductivity data analysis based on a nonlinear fit. This research will promote our basic understanding of the aggregation behavior of $[C_n mpy][Br]$ in water.

2 Experimental

2.1 Materials

3-methylpyridinium (97%), 1-bromododecane (97%), 1-bromotetradecane (97%), 1-bromohexadecane (97%), toluene (99%), ethyl acetate (97%), ethanol (99%), *n*-propanol (99%), *n*-butanol (99%), and *n*-pentanol (99%), pyrene (97%), lithium bromide (LiBr analytical reagents, ≥99%), sodium bromide (NaBr analytical reagents, ≥99%), magnesium bromide (MgBr$_2$ analytical reagents, ≥99%), was obtained from Macklin Reagent. Dilute stock solutions of pyrene (1×10^{-3} mol L^{-1}) were prepared by dissolving pyrene in methanol in a volumetric flask. Samples for UV were prepared as follows: equivalent amounts of probe stock solutions were transferred into test tubes and evaporated with nitrogen. Then the ILs solution was added.

2.2 Instrumentation

Confirmation of the structures of $[C_n mpy][Br]$ was obtained by infrared spectroscopy (FTIR) and nuclear magnetic resonance (NMR). FTIR spectra (KBr) were recorded in the 4000–400 cm^{-1} range on a Lambda 7600 s FT-IR spectrometer (Lambda, Australia). ^{1}H, ^{13}C NMR spectra were recorded on a Bruker Avance 400 nuclear magnetic resonance (Bruker, Switzerland) operating at 400 and 100 MHz respectively with CDCl$_3$ as a solvent, and tetramethylsilane (TMS) as an internal standard.

2.3 Synthesis

$[C_{12} mpy][Br]$ were synthesized according to a previously reported procedure.[33] Briefly, equimolar amounts (0.1 mol) of 3-methylpyridinium and 1-bromododecane were mixed in 30 mL dry toluene in a 100 mL three-necked flask and refluxed for 6 h under nitrogen atmosphere. After the reaction, toluene was removed under vacuum and the pure $[C_{12} mpy][Br]$ was recrystallized in fresh ethyl acetate at least four times. The syntheses of $[C_{14} mpy][Br]$ and $[C_{16} mpy][Br]$ are very similar to the above procedure, in which 1-bromotetradecane and 1-bromohexadecane were used, respectively. The synthetic pathways of the surfactants are shown in Fig. 1.

These synthesized surfactants were characterized by ^{1}H, ^{13}C NMR and FTIR spectra, the detailed spectroscopic data were in
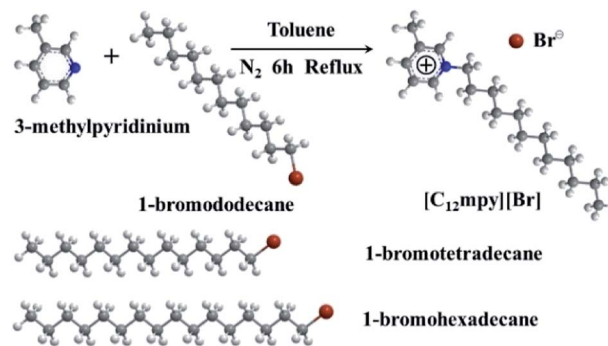

Fig. 1 The synthetic pathways of $[C_n mpy][Br]$ (n = 12, 14, 16).

ESI, Fig. S1† shows (^{1}H, ^{13}C) NMR and FTIR spectra of synthesised $[C_n mpy][Br]$.

2.4 Surface tension measurements

The surface tension of ILs solutions were measured with a Du Noüy tensiometer (Krüss K100, Germany) by applying the platinum ring technique. The surface tension recorded was related to the force required to lift the ring from the surface of the air–liquid interface.[37] Measurements were performed at 298.15 ± 0.10 K until successive values agreed to within 0.2 mN m^{-1}.

2.5 Conductivity measurements

The conductivity of the ILs solutions was measured by conductometer (DDS-307, Shanghai Precision & Scientific Instruments, China). A super-thermostatic cistern (temperature fluctuation: ±0.01 K, SC-30, Shanghai Guning Industrial Co., Ltd, China) was used to control the temperature. The conductivity measurements were carried out at different temperatures for each ILs system.

2.6 Ultraviolet absorption spectra

The UV absorption of the ILs solutions were measured on a T-6 ultraviolet-visible spectrophotometer (Beijing Purkinje General Instrument Co. Ltd. China the spectra of the samples were scanned from 220 nm to 400 nm). Pyrene (1.0×10^{-4} mol L^{-1}) was used as absorption probe. These spectra were recorded against a blank of ILs solutions, and the CMC values can be obtained from the curves of absorption intensity *versus* concentration of ILs solutions.

2.7 Surface chemical parameter calculation

Adsorption efficiency (pC_{20}). The adsorption efficiency (pC_{20}) is calculated using the following equation:

$$pC_{20} = -\lg C_{\pi=20} \tag{1}$$

In this equation, pC_{20} is the negative log of the ILs surfactants concentration which reduce the surface tension of the pure solvent by 20 mN m^{-1}.[22,23,38]

Effectiveness of surface tension reduction (Π_{cmc}). To show the ability to decrease surface tension of solutions, the effectiveness of the surface tension reduction (Π_{cmc}) is defined as:

$$\Pi_{cmc} = \gamma_0 - \gamma_{cmc} \tag{2}$$

where γ_0 is the surface tension of bidistilled water and γ_{cmc} is the surface tension of the solutions at CMC.[22,23,38]

Maximum surface excess concentration (Γ_{max}). The maximum surface excess concentration (Γ_{max}) at the air/water interface was estimated by applying Gibbs adsorption isotherm:

$$\Gamma_{max} = -\frac{1}{2.303nRT}\left(\frac{d\gamma}{d\log C}\right)_{T,P} \tag{3}$$

where, R is the gas constant (8.314 J mol^{-1} K^{-1}), T is the absolute temperature and C is the surfactant concentration. As there is one counter ion associated with one ionic head group, the value of n is taken to be 2.[18,20,38]

Minimum surface area (A_{min}). Minimum surface area (A_{min}) provides information on the degree of packing and orientation of the adsorbed surfactant molecule. The minimum area occupied by a single amphiphilic molecule at the air–water interface (A_{min}) was calculated by applying the Gibbs adsorption isotherm:

$$A_{min} = \frac{1}{N_A \Gamma_{Max}} \tag{4}$$

where N_A is the Avogadro constant.[20,38]

3 Results and discussion

3.1 The CMC of [C$_n$mpy][Br]

The aggregation behavior of the three surfactants aqueous solutions was studied *via* conductivity measurements. As far as the conductivity measurements are concerned, the CMC values were obtained at the point of intersection of the linear portions of conductivity *versus* concentration plots above and below the breakpoint. Here, we used a different approach in the conductivity data analysis based on a nonlinear fit introduced by Carpena *et al.*[39] to determine common micellization parameters of ILs, such as CMC value and the degree of dissociation of micelles (β). This method was successfully applied to analyze conductivity data on several surfactants.[10,30,40,41] The conductivity data were fitted by the function reported in eqn (5), which represents the integral function of a sigmoid:

$$\kappa(c) = \kappa(0) + A_1 c + \Delta c(A_2 - A_1)\ln\left(\frac{1+e^{(c-c_0)/\Delta c}}{1+e^{-c_0/\Delta c}}\right) \tag{5}$$

where κ_0 is the initial conductivity of water, A_1 and A_2 are the limiting slopes for low and high concentration respectively, C_0 is the central point of the transition (*i.e.* CMC value) and ΔC is the width of the transition. The β value can be deduced from the ratio A_2/A_1. The variations of conductivity against concentration of ILs at 298.15 K are shown in Fig. 2.

As shown in Fig. 2, it is obvious that a trend changes of rapid rise and then slow rise appeared in the curves with the increase of ILs concentration. The conductivity of the solution rising
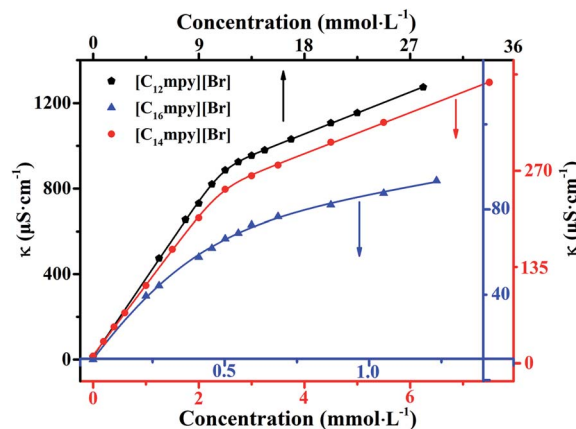

Fig. 2 Conductivity dependence of concentration for [C$_n$mpy][Br] in aqueous solution at 298.15 K.

rapidly in the pre-micellar region. This is due to the concentration of current carriers increased with the rising of ILs concentration. Due to binding of a fraction of the counterions to the micellar surface resulting in an effective loss of ionic charges, and a slower rise in the isotherm area of electrical conductivity after micellization.[26] Moreover, the proposed function will accurately represent the physical model to which the conductivity data would adhere. This method avoids any data processing and thus avoids the introduction of noise. By using nonlinear fit simply search for the best correlation, the evaluation of the degree of counterion binding β could be performed, avoiding artifacts due to the individual selection of points to be included in the linear fit of the linear regimes.

The surface tension measurement is a classical method in studying the CMC of surfactants. The variations of the surface tension (γ) with the ILs concentration (C) at 298.15 K are shown in Fig. 3. The plots of γ *versus* log C show a breakpoint concentration corresponding to the CMC value of the three surfactants. The CMC values are listed in Table 1.
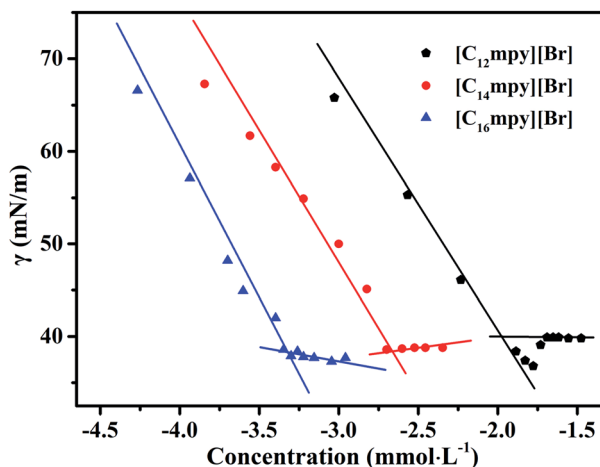

Fig. 3 Surface tension *vs.* concentration plot of [C$_n$mpy][Br] in aqueous solution at 298.15 K.

Table 1 The values of CMC determined by conductivity measurement, surface tension and UV absorption spectra for the $[C_n mpy][Br]$ in aqueous solution at 298.15 K

ILs	CMC (mmol L^{-1})		
	Conductivity measurements	Surface tension	Ultraviolet absorption
$[C_{12}mpy][Br]$	9.74	9.83	10.04
$[C_{14}mpy][Br]$	2.40	2.26	2.33
$[C_{16}mpy][Br]$	0.567	0.508	0.520

As shown in Fig. 3, surface tension values decrease rapidly with increasing surfactant concentration due to the adsorption of molecules at the air–liquid interface. Then a distinct break point appears, indicating the formation of micelles.[19] The CMC value was determined from the break point of the plot. After the break point, the surface tension remains nearly constant with increasing ILs concentrations. This is due to the saturation of the air–liquid interface with ILs molecules.[37]

The UV spectrometric technique is also an easy method to determine the CMC of surfactants.[42,43] In this method, pyrene was used as absorption probe. The maximum characteristic absorption wavelength (λ_{max}) of pyrene was determined by plotting the absorption intensity of pyrene $vs.$ wavelength, which was 338 nm. Subsequently, the CMC values were measured by plotting absorption intensity $vs.$ various concentrations of ILs solutions containing pyrene at 338 nm. Fig. S2† shows the absorbance plots affected by varying concentrations of $[C_n mpy][Br]$ ($n = 12, 14, 16$) containing pyrene in aqueous solution. In polar region, the intensity of the peaks enhanced slowly, while the absorption intensity enhanced dramatically when the microenvironment changed. Thus, the abrupt change on the curve of absorption intensity $vs.$ concentration indicated the formation of micelles.[44] Fig. 4 shows the plots of absorption intensity $vs.$ concentration of $[C_n mpy][Br]$ at 338 nm. The CMC values of $[C_n mpy][Br]$ with different chain length obtained from the three methods mentioned above are listed in Table 1.
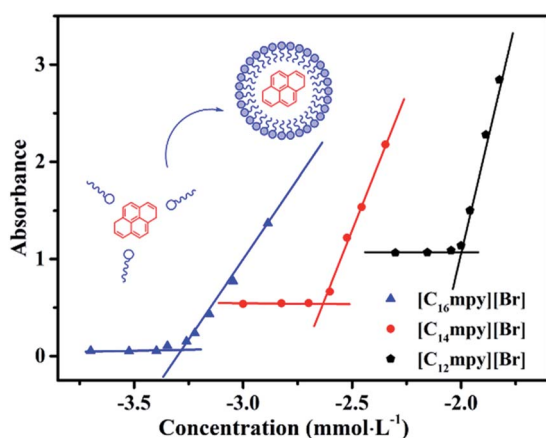

Fig. 4 The plots of absorption intensity $vs.$ concentration of $[C_n mpy]$[Br] at 338 nm.

3.2 Surface activity of $[C_n mpy][Br]$

The surface properties of the surfactants including the CMC, surface tension (γ_{cmc}), the maximum surface pressure (Π_{cmc}), adsorption efficiency (pC_{20}), maximum surface excess concentration (Γ_{max}), and the minimum surface area (A_{min}) are listed in Table 2, together with the data reported for dodecyltrimethyl ammonium bromide (DTAB), tetradecyltrimethyl ammonium bromide (TTAB), cetyltrimethyl ammonium bromide (CTAB) and n-alkyl-pyridinium bromide ($[C_n py][Br]$, $n = 12, 14, 16$).

From the obtained results, all the synthesized surfactants show moderate surface activity. It is obvious that surface tension (γ_{cmc}) decrease from 39.2 to 37.6 mN m^{-1}, which is due to the increased hydrophobic nature of the ILs. The CMC values of ILs are compared with those of DTAB, TTAB, CTAB and $[C_n py]$ [Br] ($n = 12, 14, 16$) in Table 2. It is observed that CMC values of ILs are lower in comparison to these conventional cationic surfactants and $[C_n py][Br]$. The CMC values of ILs gradually decrease as the hydrophobic chain length increases from 12 to 16. This indicates a relationship between CMC value and alkyl chain length of ILs, that is, the longer the alkyl chain is, the lower CMC value will be. Two important parameters of surfactants, $i.e.$ the effectiveness of surface tension reduction (Π_{CMC}) and the adsorption efficiency (pC_{20}) were obtained from the surface tension plots. The maximum reduction in surface tension caused by the dissolution of amphiphilic molecules has been indicated by Π_{CMC} and as a result Π_{CMC} becomes a symbol for the effectiveness of the amphiphile to lower the surface tension of the water.[50] Pyridinium-based surfactants synthesized in present work have greater ability to reduce surface tension of the aqueous system. pC_{20}, generally used to indicate the efficiency of surfactant to decrease surface tension of water or other solvent, is found to increase in the order of $[C_{12}mpy]$ [Br] < $[C_{14}mpy][Br]$ < $[C_{16}mpy][Br]$. Comparing with conventional surfactants, $[C_n mpy][Br]$ show better surface activity. The ratio of CMC/C_{20} can evaluate the structural factors and various microenvironments in the process of adsorption or micellization.[37] The greater the CMC/C_{20} is, the greater tendency of the amphiphile has to reduce surface tension of the system. Thus, $[C_{12}mpy][Br]$ have a strong ability to reduce surface tension of aqueous system, while the corresponding ability of $[C_{14}mpy][Br]$ and $[C_{16}mpy][Br]$ is weaker. The maximum surface excess concentration (Γ_{max}) and the minimum surface area (A_{min}), two additional important parameters of surfactants which reflect the molecular arrangement of ILs molecules at the air–liquid interface, were estimated by Gibbs adsorption isotherm. Table 2 shows an increasing trend in Γ_{max} and decreasing A_{min} values. This indicates that the ILs with longer alkyl chains have higher hydrophobicity, leading to greater adsorption of more molecules at the interface. The greater the adsorption, the smaller the effective area (A_{min}) of the ILs molecules at the surface is. ILs molecules with longer alkyl chains form more compact monolayers that occupy less area.[37] It is interesting to find that the trend for Γ_{max} value of $[C_n mpy][Br]$ is opposite to $[C_n py][Br]$, although $[C_n mpy][Br]$ possess a much larger headgroup. This result may be due to the more dispersed charge of the $[C_n mpy]^+$ cation, which could weaken the electrostatic repulsion among

Table 2 Surface active properties of the synthesized surfactants

ILs	CMC (mmol L^{-1})	pC_{20}	γ_{cmc} (mN m^{-1})	A_{min} (nm^2)	Γ_{max} (μmol m^{-2})	Π_{cmc} (mN m^{-1})	CMC/C_{20}
[C$_{12}$mpy][Br]	9.83	2.8	39.2	0.903	1.84	32.9	6.22
[C$_{14}$mpy][Br]	2.26	3.1	38.8	0.794	2.09	33.3	2.86
[C$_{16}$mpy][Br]	0.508	3.8	37.6	0.697	2.38	34.5	3.22
[C$_{12}$py][Br]	10.0 (ref. 46)	2.3 (ref. 47)	39.3 (ref. 26)	0.71 (ref. 26)	2.34 (ref. 26)	32.93 (ref. 47)	2.53 (ref. 47)
[C$_{14}$py][Br]	2.70 (ref. 46)	—	38.0 (ref. 26)	0.86 (ref. 26)	1.93 (ref. 26)	—	—
[C$_{16}$py][Br]	0.64 (ref. 46)	2.7 (ref. 48)	44.0 (ref. 48) 45.0 (ref. 49)	1.26 (ref. 48)	1.32 (ref. 48)	28.5 (ref. 48)	—
DTAB[45]	12.45	2.1	—	0.476	3.49	32.4	1.57
TTAB[45]	3.60	2.9	—	0.514	2.09	32.9	2.86
CTAB[45]	0.89	3.2	—	0.459	3.62	28.1	1.41

head groups.[19] In addition, for [C$_n$mpy][Br], the relationship of minimum surface area per amphiphilic molecule *versus* the number of carbon atoms in the alkyl chain is linear, which can be described by $a_0 = 1.519 - 0.0515n$.

3.3 Effect of additives on micellization of [C$_n$mpy][Br]

As is well known, the aggregation formation of surfactants in water can be observably affected by the nature of additives presented in solution.[51] Therefore, it is very important to study the effect of additives on the CMC value of surfactants in both theory and practice.

As can be seen from Table 3, the effect of inorganic salts and organic alcohols on the CMC value of ILs show the same trend. It is obvious that the CMC value decrease when inorganic salts were presented in ILs aqueous solution. Fig. S3 to S9† showed the electrical conductivities plots affected by inorganic salts and different organic alcohols in varying concentrations of [C$_n$mpy][Br] (*n* = 12, 14, 16) aqueous solution. This phenomenon can be explained as the counterion effect. In general, aggregation formation for surfactants is dictated by a balance between the repulsive headgroup interactions and the attractive forces to

arising from a need to minimize the exposure of the hydrophobic core to water.[28] Increasing amount of counterions will alter the two forces. As a result, adsorption of the counterions onto the aggregates surface can reduce the repulsive between pyridine head group of [C$_n$mpy][Br], thereby lowering the CMC values of the [C$_n$mpy][Br]. Moreover, it is found that cations had an insignificant effect on the CMC value.

The CMC value of ILs tends to increase slightly with added ethanol, and decrease gradually when *n*-propanol, *n*-butanol and *n*-pentanol are added. In general, the polar organic molecular affects the properties of surfactants by protecting or destroying the structure of water surrounding the hydrophobic chains. Ethanol is solubilized mainly in water and "palisade layer" of micelle aggregates formed by ILs molecules,[52] which destroying the "iceberg structure" surrounding the hydrophobic chains of surfactant molecules, weakening the hydrophobic effect and the ability of micellization of surfactants. Thereby the CMC value tend to increase slightly. However, with the increase of alkyl chain length of additive alcohol, the CMC values decrease gradually because of two reasons: (i) the solubility of alcohol in water decreases, forming the "iceberg structure"

Table 3 The values of CMC for system in the solution of water added inorganic salt and organic alcohols (the molarity of inorganic salt is 0.20 mmol L^{-1}, MgBr$_2$ is 0.10 mmol L^{-1}, the mass fraction of alcohols is 1%) at different temperatures

| ILs	T (K)	CMC (mmol L^{-1})							
		No additive	LiBr	NaBr	MgBr$_2$	C$_2$H$_5$OH	C$_3$H$_7$OH	C$_4$H$_9$OH	C$_5$H$_{11}$OH
[C$_{12}$mpy][Br]	298.15	9.74	9.18	9.17	9.23	9.83	9.38	8.24	5.94
	303.15	9.77	9.30	9.23	9.42	9.92	9.46	8.26	5.80
	308.15	10.02	9.58	9.32	9.79	10.14	9.70	8.47	5.91
	313.15	10.54	10.03	9.70	10.11	10.56	9.98	8.64	5.95
	318.15	11.47	10.30	10.56	10.80	11.82	10.48	8.84	6.26
[C$_{14}$mpy][Br]	298.15	2.40	1.56	1.53	1.77	2.48	2.30	2.10	1.48
	303.15	2.45	1.67	1.68	1.88	2.56	2.38	2.18	1.42
	308.15	2.51	1.88	1.82	1.93	2.66	2.49	2.29	1.50
	313.15	2.81	2.08	2.08	2.15	2.84	2.67	2.36	1.69
	318.15	2.84	2.17	2.23	2.26	2.91	2.78	2.48	1.93
[C$_{16}$mpy][Br]	298.15	0.567	0.502	0.474	0.348	0.575	0.476	0.466	0.453
	303.15	0.590	0.513	0.513	0.349	0.596	0.503	0.498	0.473
	308.15	0.597	0.531	0.536	0.354	0.613	0.591	0.541	0.528
	313.15	0.647	0.541	0.597	0.362	0.665	0.657	0.568	0.572
	318.15	0.668	0.570	0.609	0.384	0.690	0.668	0.596	0.576
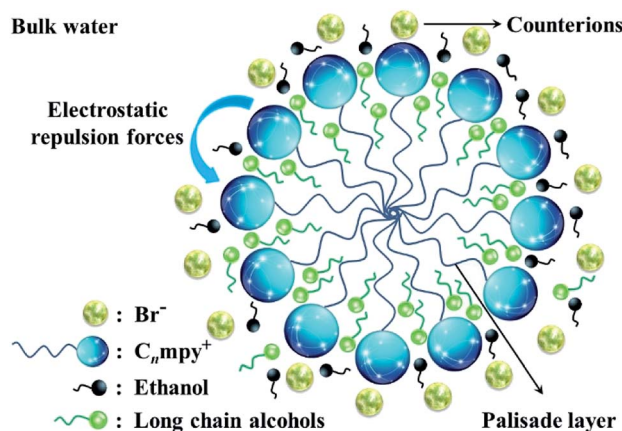
Fig. 5 Schematic illustration of [$C_n$mpy][Br] micelle in the presence of inorganic salts and organic alcohols in water.

around the long chain alcohol molecules. This effect is beneficial to the participation of long chain alcohols in the micellization process. (ii) The long chain alcohol molecules can also insert into the palisade layer, which can decrease the electrostatic repulsion forces of ionic head-groups in the micelle,[21] this effect caused by long chain alcohols corresponded to that of cosurfactants. Both of above reasons justified the lower CMC values when the additives were *n*-propanol, *n*-butanol and *n*-pentanol. According to the analysis above and literature reports,[53–55] the possible structure of micelle in the presence of inorganic salts and organic alcohols in water was depicted and shown in Fig. 5.

3.4 Thermodynamics of micellization

Conductivities of ILs solutions are studied to estimate their micellization behavior. The variation values of CMC and β in different temperatures may be utilized to calculate the thermodynamic parameters of micelle formation. The variations of conductivity against concentration of ILs solutions at different temperatures are shown in Fig. 6. For cationic surfactants, the free energy of micellization and adsorption may be calculated by following equation:[37,38,56]

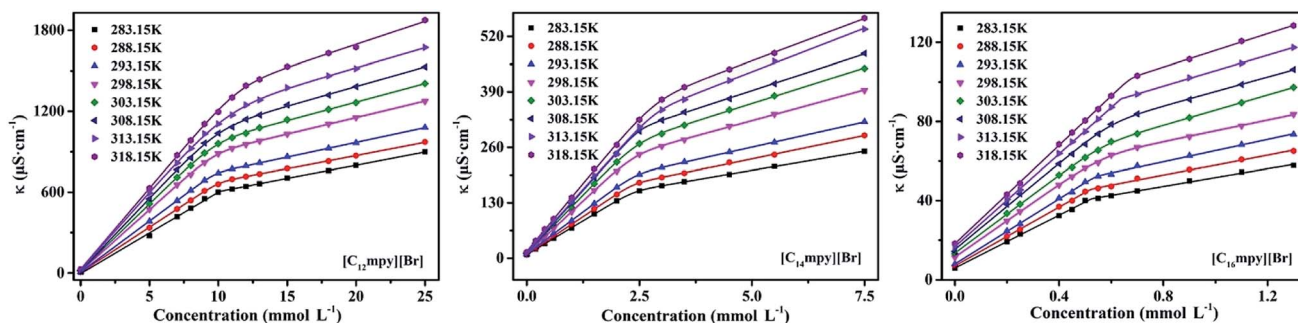$$\Delta G_m^\theta = (2 - \beta)RT \ln X_{cmc} \quad (6)$$

$$\Delta G_{ads}^\theta = \Delta G_m^\theta - \Pi_{CMC}/\Gamma_{max} \quad (7)$$

where ΔG_m^θ and ΔG_{ads}^θ are the standard Gibbs free energy changes of micellization and adsorption, respectively. β is the degree of dissociation, the gas constant $R = 8.314$ J mol^{-1} K^{-1}, T is the absolute temperature, X_{cmc} is CMC in mole fraction; X_{cmc} = CMC/55.4, where CMC is in mol L^{-1} and the factor 55.4 accounts for the fact that 1 L of water corresponds to 55.4 mol of water at 298.15 K.

The enthalpy of micellization (ΔH_m^θ) can be determined by using the Gibbs–Helmholtz equation:[21,38]

$$\Delta H_m^\theta = -2.3 \times (2 - \beta)RT^2 \left[\frac{\partial(\log \chi_{CMC})}{\partial T} \right] \quad (8)$$

The term $(\partial \log X_{cmc}/\partial T)_P$ was calculated by fitting a second order polynomial to the log X_{cmc} *versus* temperature plots and by taking the corresponding temperature derivative.[57] The coefficients of polynomials are given in Table 1S in ESI.†

Finally, the standard entropy change during the micelle formation, ΔS_m^θ is calculated using eqn (9):

$$\Delta S_m^\theta = \frac{\Delta H_m - \Delta G_m}{T} \quad (9)$$

The thermodynamic parameters for ILs at different temperatures are listed in Table 4. As can be seen from Table 4, the changes of the free energy of adsorption (ΔG_{ads}^θ) and micellization (ΔG_m^θ) are all negative, indicating a spontaneous process of micellization and adsorption in water. A higher magnitude of ΔG_{ads}^θ is observed as compared to ΔG_m^θ values, showing that adsorption process favorably occurs until all the air/solution interface is occupied, and then surfactants molecules begin to aggregate and form micelles in the bulk solution.[58,59] ΔG_m^θ and ΔG_{ads}^θ become more negative with increasing alkyl chain length or solution temperature. This may be due to the increased hydrophobicity of ILs, which can destroy the structure of water and increase free energy of the system, and improve the propensity of ILs molecules to migrate to the interface. This behavior can make energy of the surfactant system decrease. Thus the values of ΔG_m^θ and ΔG_{ads}^θ are more negative.[59] Rising temperature can cause the decrease of hydration around hydrophilic groups, which results in the increase of the system

Fig. 6 Conductivity dependence of concentration for [$C_n$mpy][Br] in aqueous solution at different temperature.

Table 4 The values of CMC and β, and thermodynamic parameters for $[C_n mpy][Br]$ in aqueous solution at different temperatures

ILs	T (K)	CMC (mmol L^{-1})	β	ΔG_m^θ (kJ mol^{-1})	ΔH_m^θ (kJ mol^{-1})	ΔS_m^θ (kJ mol^{-1} K^{-1})	$T\Delta S_m^\theta$ (kJ mol^{-1})	ΔG_{ads}^θ (kJ mol^{-1})
$[C_{12}mpy][Br]$	283.15	9.93	0.303	−34.46	6.194	0.1436	40.65	
	288.15	9.82	0.300	−35.18	2.918	0.1322	38.10	
	293.15	9.76	0.287	−36.09	−0.616	0.1210	35.47	
	298.15	9.74	0.268	−37.12	−4.472	0.1095	32.65	−55.00
	303.15	9.77	0.274	−37.60	−8.550	0.09583	29.05	
	308.15	10.02	0.270	−38.20	−12.94	0.08197	25.26	
	313.15	10.54	0.258	−38.85	−16.70	0.07073	22.15	
	318.15	11.47	0.240	−39.49	−19.69	0.06223	19.80	
$[C_{14}mpy][Br]$	283.15	2.37	0.311	−39.99	2.585	0.1504	42.58	
	288.15	2.35	0.309	−40.79	−0.138	0.1411	40.65	
	293.15	2.38	0.295	−41.78	−3.082	0.1320	38.70	
	298.15	2.40	0.295	−42.46	−6.237	0.1215	36.22	−58.39
	303.15	2.45	0.301	−42.93	−9.560	0.1101	33.37	
	308.15	2.51	0.302	−43.51	−13.11	0.09865	30.40	
	313.15	2.81	0.285	−44.16	−17.05	0.08657	27.11	
	318.15	2.84	0.285	−44.81	−21.08	0.07458	23.73	
$[C_{16}mpy][Br]$	283.15	0.527	0.324	−45.62	0.5005	0.1629	46.12	
	288.15	0.523	0.322	−46.52	−0.7750	0.1556	45.75	
	293.15	0.540	0.317	−47.33	−2.148	0.1541	45.18	
	298.15	0.567	0.297	−48.50	−3.653	0.1503	44.85	−63.00
	303.15	0.590	0.307	−48.86	−5.237	0.1439	43.62	
	308.15	0.597	0.303	−49.73	−6.884	0.1390	42.85	
	313.15	0.647	0.298	−50.33	−8.681	0.1330	41.95	
	318.15	0.668	0.295	−51.08	−10.58	0.1273	40.50	

energy, improves profitably to adsorption in the interface and formation of micelles in order to decrease energy of the surfactant system.[16,37,38] The enthalpy of $[C_{12}mpy][Br]$ is negative at 293.15 K and becomes negative with temperature increase, for the $[C_{14}mpy][Br]$ and $[C_{16}mpy][Br]$ this transition occurs at 288.15 K, implying that the micelle formation process is endothermic at lower temperatures and exothermic at higher temperatures. This behavior can be attributed to the delicate balance between hydrophobic hydration of nonpolar parts (endothermic) and counterion binding (exothermic) upon micellization.[60,61] The hydrophobic effect is related to the water removal from the nonpolar surface in order to diminish the extent of less favorable hydrophobic hydration in comparison to clustered water in the bulk.[62] In the case of micellization, water molecules are organized around nonpolar surfactant tails at low temperature (they form an iceberg structure, or their dynamics is slowed down significantly at least).[63] Therefore, the destruction of this water structure is a highly endothermic process.[64] Although the formation of favorable H-bond in the bulk, ion condensation *etc.* counteract the endothermic contribution of the hydrophobic dehydration, the results of micellization are a slightly positive overall enthalpy change. In addition, water structure at the hydrophobic surfaces is at least partially disturbed at high temperature, therefore, the endothermic contribution of the hydrophobic dehydration to the micellization is smaller and ultimately the micellization becomes an exothermic process.[65] For $[C_n mpy][Br]$, the value of the standard entropy of micellization ($T\Delta S_m^\theta$) is larger than the value of enthalpy changes ($-\Delta H_m$), indicating that the entropy gain greatly affects the associated micellization process, and that the micellization for the ILs in aqueous solution is entropy-driven.[17,21,37,58] In addition, we have also found that the temperature dependence of CMC shows typical U-shaped reaching the minimum value CMC* at the temperature T^* form (Fig. S10) in ESI.† These values, obtained from the corresponding derivative of the polynomial $CMC = A + BT + CT^2$ are listed in Table 1S in ESI.† As can be seen from Table 1S,† T^* is close to temperature T_0, where $\Delta H_m^\theta = 0$.[60,61,66] The variation of CMC values of $[C_n mpy][Br]$ with temperature could be attributed to that temperature increase causes decreased hydration of hydrophilic ionic head-groups, which facilitates micellization. Whereas, temperature increase also causes disruption of the structured water surrounding the hydrophobic alkyl chains, an effect that hinders micellization.[21]

4 Conclusions

In the present work, the micellization behavior and surface activity of $[C_n mpy][Br]$ ($n = 12, 14, 16$) in aqueous solution were investigated by conductivity, surface tension and UV absorption spectra in detail. It can be concluded that $[C_n mpy][Br]$ have better surface activities than those conventional surfactants with the same alkyl chain length. The addition of inorganic salts and organic alcohol was found to exert a remarkable influence on the micellization behavior of $[C_n mpy][Br]$ in aqueous solutions. The CMC values of all the systems decreased drastically in the presence of inorganic salts. The CMC values increased slightly in the presence of ethanol, but decreased gradually with long chain alcohols. The CMC values assumed a trend of

decreases and then increases with the increase of temperature. The analysis of thermodynamic parameters indicated that both processes of adsorption and micellization of [$C_n$mpy][Br] are spontaneous, the micelle formation process is endothermic at lower temperatures and exothermic at higher temperatures. and that the micellization processes of these surfactants are entropy-driven in the investigated temperature range. Both adsorption and micellization of [$C_n$mpy][Br] are inclined to occur with the increase of alkyl chain length or temperature.

Conflicts of interest

There are no conflicts to declare.

Acknowledgements

References

1 Z. M. Xue, L. Qin, J. Y. Jiang, T. C. Mu and G. H. Gao, *Phys. Chem. Chem. Phys.*, 2018, **20**, 8382–8402.

2 Z. Q. He and P. Alexandridis, *Phys. Chem. Chem. Phys.*, 2015, **17**, 18238–18261.

3 P. C. Marr and A. C. Marr, *Green Chem.*, 2016, **18**, 105–128.

4 M. T. Mara, G. Freire, B. Saramago, J. A. P. Coutinho, J. N. C. Lopes and L. P. Rebelo, *Chem. Soc. Rev.*, 2012, **41**, 829–868.

5 L. Q. Peng, W. Y. Yu, J. J. Xu and J. Cao, *Food Chem.*, 2018, **239**, 1075–1084.

6 S. M. Ali, K. M. Emran and M. Messali, *Prog. Org. Coat.*, 2019, **130**, 226–234.

7 M. Matandabuzo and P. A. Ajibade, *J. Mol. Liq.*, 2018, **268**, 284–293.

8 M. Sabbaghan, A. S. Shahvelayati and K. Madankar, *Spectrochim. Acta, Part A*, 2015, **135**, 662–668.

9 D. H. Zhao, Y. N. Wang, E. H. Duan and J. Zhang, *Fuel Process. Technol.*, 2010, **91**, 1803–1806.

10 I. R. Palmeiro, I. R. Escontrela, O. Rodríguez, A. Arce and A. Soto, *RSC Adv.*, 2015, **5**, 37392–37398.

11 M. A. Ilies, W. A. Seitz, I. Ghiviriga, B. H. Johnson, A. Miller, E. B. Thompson and A. T. Balaban, *J. Med. Chem.*, 2004, **47**, 3744–3754.

12 M. Boukherissa, F. Mutelet, A. Modarressi, A. Dicko, D. Dafri and M. Rogalski, *Energy Fuels*, 2009, **23**, 2557–2564.

13 O. A. E. Seoud, A. Koschella, L. C. Fidale, S. Dorn and T. Heinze, *Biomacromolecules*, 2007, **8**, 2629–2647.

14 L. M. Gonçalves, T. G. Kobayakawa, D. Zanette, H. Chaimovich and I. M. Cuccovia, *J. Pharm. Sci.*, 2009, **98**, 1040–1052.

15 M. E. Jiménez, A. O. Ortega, R. P. Weigand, M. M. R. Tejada and R. P. Carpio, *Macromol. Mater. Eng.*, 2003, **288**, 945–950.

16 T. Singh and A. Kumar, *J. Phys. Chem. B*, 2007, **111**, 7843–7851.

17 N. V. Sastry, N. M. Vaghela and V. K. Aswal, *Fluid Phase Equilib.*, 2012, **327**, 22–29.

18 J. Bowers, C. P. Butts and P. J. Martin, *Langmuir*, 2004, **20**, 2191–2198.

19 L. J. Shi, N. Li, H. Yan, Y. A. Gao and L. Q. Zheng, *Langmuir*, 2011, **27**, 1618–1625.

20 J. J. Jiao, B. Dong, H. N. Zhang, Y. Y. Zhao, X. Q. Wang, R. Wang and L. Yu, *J. Phys. Chem. B*, 2012, **3**, 958–965.

21 Y. Wei, F. Wang, Z. Q. Zhang, C. C. Ren and Y. Lin, *J. Chem. Eng. Data*, 2012, **59**, 1120–1129.

22 H. Ma, H. C. Ke, T. Wang, J. H. Xiao, N. Du and L. Yu, *J. Mol. Liq.*, 2017, **240**, 556–563.

23 M. W. Zhao and L. Q. Zheng, *Phys. Chem. Chem. Phys.*, 2011, **13**, 1332–1337.

24 C. L. Dai, M. Y. Du, Y. F. Liu, S. L. Wang, J. H. Zhao, A. Chen, D. X. Peng and M. W. Zhao, *Molecules*, 2014, **19**, 20157–20169.

25 I. Bandrés, S. Meler, B. Giner, P. Cea and C. Lafuente, *J. Solution Chem.*, 2009, **38**, 1622–1634.

26 A. Cornellas, L. Perez, F. Comelles, I. Ribosa, A. Manresa and M. T. Garcia, *J. Colloid Interface Sci.*, 2011, **355**, 164–171.

27 E. A. M. Gad, M. M. A. E. Sukkary and E. M. S. Azzam, *Monatsh. Chem.*, 1997, **128**, 1237–1246.

28 H. Y. Wang, J. J. Wang, S. B. Zhang and X. P. Xuan, *J. Phys. Chem. B*, 2008, **112**, 16682–16689.

29 T. Singh and A. Kumar, *Colloids Surf., A*, 2008, **318**, 263–268.

30 P. Quagliotto, N. Barbero, C. Barolo, E. Artuso, C. Compari, E. Fisicaro and G. Viscardi, *J. Colloid Interface Sci.*, 2009, **340**, 269–275.

31 N. V. Sastry, N. M. Vaghela, P. M. Macwan, S. S. Soni, V. K. Aswal and A. Gibaud, *J. Colloid Interface Sci.*, 2012, **371**, 52–61.

32 A. Tiwari, M. Sahoo, P. Soreng and B. K. Mishra, *J. Surfactants Deterg.*, 2018, **21**, 367–373.

33 S. Fayyaz, S. Ali, N. Khalid, A. Shah and F. Ullah, *J. Surfactants Deterg.*, 2016, **19**, 841–848.

34 S. Fayyaz, R. Talat, S. Ali, N. Khalid, A. Shah and F. Ullah, *J. Surfactants Deterg.*, 2019, **22**, 625–632.

35 M. M. Knock and C. D. Bain, *Langmuir*, 2000, **16**, 2857–2865.

36 V. Pino, C. Yao and J. L. Anderson, *J. Colloid Interface Sci.*, 2009, **333**, 548–556.

37 G. Z. Cao, X. F. Guo, L. H. Jia and X. H. Tian, *RSC Adv.*, 2015, **5**, 27197–27204.

38 L. Qin and X. H. Wang, *RSC Adv.*, 2017, **7**, 51426–51435.

39 P. Carpena, J. Aguia, B. Galván and C. C. Ruiz, *Langmuir*, 2002, **18**, 6054–6058.

40 P. Quagliotto, G. Viscardi, C. Barolo, E. Barni, S. Bellinvia, E. Fisicaro and C. Compari, *J. Org. Chem.*, 2003, **68**, 7651–7660.

41 H. L. Zhu, Z. Y. Hu, X. M. Ma, J. L. Wang and D. L. Cao, *J. Surfactants Deterg.*, 2016, **19**, 265–274.

42 H. Suzuki, *J. Am. Oil Chem. Soc.*, 1970, **47**, 273–277.

43 M. K. Banjare, K. Behera, M. L. Satnami, S. Pandey and K. K. Ghosh, *RSC Adv.*, 2018, **8**, 7969–7979.

44 A. Dominguez, A. Fernandez, N. Gonzalez, E. Iglesias and L. Montenegro, *J. Chem. Educ.*, 1997, **74**, 1227–1231.

45 X. J. Qi, X. L. Zhang, G. X. Luo, C. Y. Han, C. S. Liu and S. H. Zhang, *J. Dispersion Sci. Technol.*, 2013, **34**, 125–133.

46 J. Škerjanc, K. Kogej and J. Cerar, *Langmuir*, 1999, **15**, 5023–5028.

47 M. J. Rosen, M. Dahanayake and A. W. Cohen, *Colloids Surf.*, 1982, **5**, 159–172.

48 L. R. Harutyunyan and R. S. Harutyunyan, *Tenside, Surfactants, Deterg.*, 2017, **54**, 141–159.

49 A. Zdziennicka, *Colloids Surf., A*, 2008, **325**, 93–100.

50 I. Ahmad, P. Patial, C. Kaur and S. Kaur, *J. Surfactants Deterg.*, 2014, **17**, 269–277.

51 M. F. Ahmed, M. R. Molla, M. Saha, I. Shahriar, M. S. Rahman, M. A. Halim, M. A. Rub, M. A. Hoque and A. M. Asiri, *RSC Adv.*, 2019, **9**, 6556–6567.

52 C. Gamboa, A. Olea, H. Rios and M. Henriquez, *Langmuir*, 1992, **8**, 23–26.

53 S. Mondal, S. Ghosh and S. De, *RSC Adv.*, 2015, **5**, 104493–104501.

54 P. P. Sun, L. J. Shi, F. Lua and L. Q. Zheng, *RSC Adv.*, 2016, **6**, 27370–27377.

55 P. Mukherjee, J. A. Crank, M. Halder, D. W. Armstrong and J. W. Petrich, *J. Phys. Chem. A*, 2006, **110**, 10725–10730.

56 Z. H. Asadov, R. A. Rahimov, K. A. Mammadova, A. V. Gurbanov and G. A. Ahmadova, *J. Surfactants Deterg.*, 2016, **19**, 145–153.

57 Z. Medoš and M. Bešter-Rogač, *J. Chem. Thermodyn.*, 2015, **83**, 117–122.

58 Y. C. Xie, J. Li, Z. F. Li, T. Sun, Y. P. Wang and G. M. Qu, *RSC Adv.*, 2018, **8**, 36015–36024.

59 S. F. Gao, Z. Z. Song, D. Zhu, F. Lan and Q. Z. Jiang, *RSC Adv.*, 2018, **8**, 33256–33268.

60 I. Čobanov, B. Šarac, Ž. Medoš, M. Vraneš, S. Gadžurić, N. Zec and M. Bešter-Rogač, *J. Mol. Liq.*, 2018, **271**, 437–442.

61 B. Šarac, Ž. Medoš, A. Cognigni, K. Bica, L. J. Chen and M. Bešter-Rogač, *Colloids Surf., A*, 2017, **532**, 609–617.

62 A. Kroflič, B. Šarac and M. Bešter-Rogač, *J. Chem. Thermodyn.*, 2011, **43**, 1557–1563.

63 A. Kroflič, B. Šarac, J. Cerkovnik and M. Bešter-Rogač, *Colloids Surf., A*, 2014, **460**, 108–117.

64 T. M. Perger and M. Bešter-Rogač, *J. Colloid Interface Sci.*, 2007, **313**, 288–295.

65 B. Šarac and M. Bešter-Rogač, *J. Colloid Interface Sci.*, 2009, **338**, 216–221.

66 J. Lah, M. Bešter-Rogač, T. M. Perger and G. Vesnaver, *J. Phys. Chem. B*, 2006, **110**, 23279–23291.